

## Influence of Silane-doped Argon Processing Atmosphere on Powder Recycling and Part Properties in L-PBF of Ti-6Al-4V

N. Emminghaus<sup>1\*</sup>, R. Bernhard<sup>1</sup>, J. Hermsdorf<sup>1</sup>, L. Overmeyer<sup>2</sup>, and S. Kaierle<sup>1,2</sup>

<sup>1</sup>Laser Zentrum Hannover e.V., Hollerithallee 8, 30419 Hannover, Germany

<sup>2</sup>Leibniz Universität Hannover, Institut für Transport- und Automatisierungstechnik, An der Universität 2,  
30823 Garbsen, Germany

\*Corresponding author: n.emminghaus@lzh.de

### Abstract

In the additive manufacturing of metal powders, the residual oxygen in the processing atmosphere plays a crucial role, especially in highly reactive materials like titanium alloys. Besides oxidation of the built parts, it leads to oxygen pick-up into the unmolten powder. Since oxidized particles cannot be removed during recycling, the powder properties deteriorate after multiple uses. In this work, Ti-6Al-4V powder was processed under conventional argon atmosphere (residual oxygen content < 0.01 vol%) as well as silane-doped argon atmosphere (< 0.001 vol% silane in argon). The silane-doping leads to a residual oxygen content of < 10<sup>-20</sup> vol%. The powder was sieved and used 5 times for each atmosphere. The powder properties morphology, chemical composition and flowability were analyzed for virgin as well as reused powder. Furthermore, the roughness and relative density of the built parts were evaluated. It was hypothesized that oxygen-free production improves recyclability and thus resource efficiency.

**Keywords:** Additive Manufacturing, Ti-6Al-4V, Laser powder bed fusion, silane, powder recycling

### Introduction

As an additive manufacturing technique, laser powder bed fusion (L-PBF) enables the fabrication of parts with intricate shapes without increasing costs for increasing geometrical complexity. Beside this, a major advantage is the theoretically high material usage of the process. Only the powder material required for the final part is molten and due to near-net-shape fabrication, little to no post-processing is necessary. However, to realize this potential, the unmolten powder must be recycled. Gas-atomized metal powders are expensive (~ 200 €/kg for Ti-6Al-4V Grade 23) and account for around 30 % of the component costs [1]. Since only 10 – 50 % of the powder is actually processed during a build job, the final part costs would be up to twice as high if no recycling would be conducted [2]. During each usage and recycling process, the powder degrades due to oxidation, spatter formation and size segregation processes [2–5]. While large spatter particles can be eliminated by sieving, smaller oxidized particles remain in the recycled powder feedstock and can represent chemical flaws in the built parts [6].

Various studies have investigated the effects of powder recycling on the powder and part properties. Due to its high reactivity and oxygen affinity, titanium and its alloys are particularly susceptible to chemical changes during processing and recycling. For the L-PBF of Ti-6Al-4V, Seyda et al. noticed powder coarsening, improved flowability as well as increased density of the built parts for recycled powder after 12 builds in comparison to virgin powder [7]. Regarding the influence on the final part properties, Seyda et al. observed an increase in hardness and ultimate tensile strength (UTS) [7]. Quintana et al., Carrion et al. and a white paper by Renishaw plc also reported changes in the particle size distribution and an improved flowability for recycled powder for the single batch recycling approach and reusing cycle numbers between 11 and 38 times [8–10]. Additionally, an increase in the powder oxygen content was observed, which has partly led to the oxygen limits for Ti-6Al-4V according to ASTM being reached or exceeded [8–10]. O’Leary et al. did not observe an increase of oxygen in the unmolten powder after 5 reusing cycles but noticed an increase of oxygen content in the built parts [11]. According to ASTM F2924-14 and ASTM F3001-14, the oxygen limit for Grade 5 and Grade 23 is 0.20 wt% and

0.13 wt%, respectively [12]. An increased oxygen content has been reported to lead to reduced impact toughness [13], increased strength [14] as well as embrittlement [15,16] and decrease of fatigue life [17]. Therefore, it is highly important to reduce powder oxidation during processing and recycling.

To minimize oxygen pick-up by the powder and built part during the L-PBF process, the most direct approach is to eliminate the residual oxygen in the processing atmosphere. It has been shown that with increasing residual oxygen content in the process atmosphere, there is also an increased pick-up of oxygen, nitrogen, and hydrogen [18]. Moreover, the oxide layer thickness increases [18]. An additional effect of reduced oxygen content in the processing atmosphere is the reduction of spattering [19], which is the main contributor to powder degradation according to Raza et al. [3,4]. However, reducing the residual oxygen content to 1000 ppm, as it is conventionally achieved in commercial systems [15,17], is not sufficient to avoid critical oxidations. According to Lee et al., the thermodynamically critical oxygen partial pressure for titanium is  $2.32 \cdot 10^{-19}$  atm [20].

A new approach to eliminate the residual oxygen content is adding small amounts of monosilane ( $\text{SiH}_4$ , hereinafter referred to as “silane”) to the inert argon processing atmosphere [21]. Silane is a highly reactive gas and reacts with the residual oxygen resulting in the formation of  $\text{SiO}_2$ ,  $\text{H}_2$  and  $\text{H}_2\text{O}$  [22,23]. With this approach, partial pressures of down to  $10^{-17}$  ppm can be achieved [21], which are adequate to an extreme high vacuum (XHV) [24]. Additionally, a previous work by the authors could show a positive side effect of the formed silicon dioxide ( $\text{SiO}_2$ ), which leads to improved flowability of the powder [25].

In this work, this new approach to a technically oxygen-free atmosphere is applied to a powder-reusing study. The powder and part properties are compared for virgin and recycled powder after 5 reusing cycles under both, argon and argon-silane atmospheres. It is hypothesized that the processing under argon-silane atmosphere leads to decreased oxidation as well as improved part properties and powder flowability.

### **Materials and Methods**

For the experiments, Ti-6Al-4V Grade 23 powder, supplied by ECKART TLS GmbH, was investigated. This powder is gas atomized and thus has a mainly spherical morphology. It has a specified particle size range of 20-53  $\mu\text{m}$ . The size distribution determined by the supplier with laser diffraction (ISO 13320) is given by the size quantiles  $D_{10} = 25.93 \mu\text{m}$ ,  $D_{50} = 38.82 \mu\text{m}$  and  $D_{90} = 57.42 \mu\text{m}$ . The Hall flowability (ASTM B213) was reported to be 33.54 s/50 g and the apparent density 2.27  $\text{g}/\text{cm}^3$  according to the supplier. Fig. 1 shows an SEM (scanning electron microscopy) image of the virgin powder. It can be seen that the particles are mostly spherical with a small amount of irregularly shaped particles and small satellites.

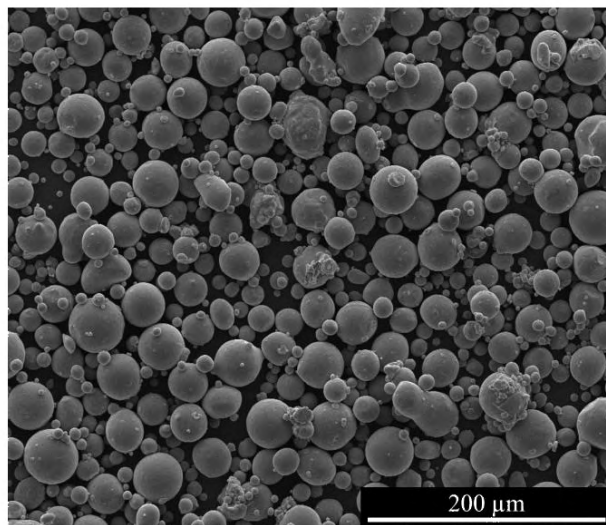


*Fig. 1: SEM image of virgin Ti-6Al-4V powder*

The powder was used for 5 build jobs under each atmosphere, i.e., pure argon and argon-silane atmosphere. After each build job, the powder was sieved under argon atmosphere with a mesh size of 53  $\mu\text{m}$ . The powder was characterized regarding its Hall flowability and apparent density before the first build job as well as after the third and fifth build job and sieving process. Analysis using SEM and EDS (energy-dispersive X-ray diffraction) was conducted for the virgin powder and after the last build job and sieving process.

A specialized laboratory machine set-up is required to conduct the L-PBF process under a silane-doped atmosphere. This is due to the reactivity of silane and the requirements regarding the handling of the reaction product silicon dioxide. Therefore, an innovative laboratory machine was developed at the Laser Zentrum Hannover e. V. (LZH), which is described in detail in a separate publication [26]. It is equipped with an ytterbium fiber laser (YLR-500-AC by IPG Laser GmbH, Germany) and the scanner system AM-Module Next Gen by Raylase GmbH, Germany. The laser emits in continuous wave mode with a maximum power of 500 W and a minimum spot diameter of 38  $\mu\text{m}$ . On this laboratory machine, experiments can be conducted in argon as well as silane-doped argon atmosphere. Due to the high gas tightness of the set-up to avoid oxygen ingress or silane leakages, a significantly lower residual oxygen content can be obtained in comparison to industrial machines. To monitor the residual oxygen content in the machine, it is equipped with a measurement and evaluation system that was developed at Clausthal University of Technology and is based on a commercial lambda sensor measurement system (Mesa Industrie-Elektronik GmbH, Marl, Germany). The gas probe extraction is situated at the top corner of the process chamber where the highest oxygen content is expected.

The layout of the conducted build jobs is displayed in Fig. 2. Geometries with a quadratic top surface (10 mm · 10 mm) and a height of 7 mm were chosen. The geometries also contain overhang sections (45 °) to enhance the imitation of application-relevant designs in which powder is trapped and experiences different heating and cooling scenarios. The specimens were built upon 3 mm columnar support structures. All specimens were manufactured with the same process parameters. A laser power of 200 W, a scanning speed of 1100 mm/s, a hatch distance of 100  $\mu\text{m}$  and a layer thickness of 30  $\mu\text{m}$  were implemented. These settings were chosen based on preliminary investigations where they led to high part quality. The hatching pattern was rotated by 67 ° between adjacent layers and no preheating of the build plate was used.

For conducting the build jobs under argon atmosphere, the machine was purged with argon 5.0 for 25 min. This leads to a residual oxygen content of 100 – 200 ppm. For establishing an XHV-adequate atmosphere a subsequent purging step with a premixed argon-silane mixture (1 vol% silane, 99 vol% argon 5.0) is added. The gas mixture is further diluted in the machine by simultaneous argon supply. This leads to a final silane content of < 0.001 vol%. Through the reaction of silane with the residual oxygen a residual oxygen content of  $10^{-20}$  vol% ( $10^{-16}$  ppm) is reached.

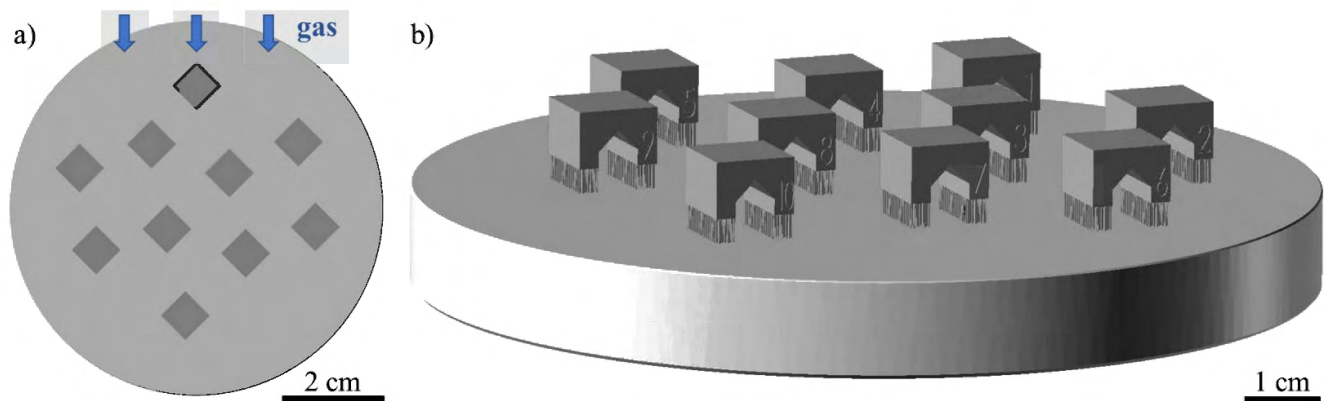


Fig. 2: Build job layout, a) top view with gas flow direction indicated by blue arrows, b) side view showing the engraved numbers, overhangs and support structures.

After build job completion, the specimens were manually taken off the build platform and cleaned with isopropanol. They were then submitted to roughness measurements. The top (horizontal) and larger side (vertical) surface were analyzed using the laser scanning confocal microscope VKX1000 by Keyence. For optical profilometry, the surface was first scanned using the focus variation function. The arithmetic mean surface roughness  $S_a$  was then determined for a measurement area of 4 mm · 4 mm. After surface characterization the specimens were embedded, ground and polished parallel to the build direction (BD). For all samples, 3 metallographic cross-sections were made. Light microscopy was employed to evaluate the relative density. For this purpose, a python script was used that calculates the ratio between black (pores) and white pixels (dense material).

## Results and Discussion

In the following, the results regarding the investigated part properties horizontal and vertical roughness and relative density as well as the powder properties Hall flowability and apparent density are described. Due to a non-optimal design of the gas flow in the system used, there was a strong accumulation of defects in the samples last scanned in each layer (sample numbers 6 - 10). These defects can override the effects of recycling grade and atmosphere on part quality. Therefore, only the first 5 samples of each build job were evaluated.

### Roughness

Concerning all build jobs, a mean horizontal roughness of 10.2  $\mu\text{m}$  and a mean vertical roughness of 12.2  $\mu\text{m}$  were obtained. Fig. 3 exemplarily shows the eight profiles of a vertical and a horizontal surface with the build direction (BD) and scan direction (SD) indicated by arrows. It can be seen that the higher vertical roughness is caused by adhering sintered particles and the effect of the single molten layers. Meanwhile, for the horizontal surface a dependence of the surface structure and roughness on the scanning strategy and scan direction can be observed. The development of the horizontal roughness as a function of the build job number is shown in Fig. 4. While higher horizontal roughness was observed for argon atmosphere in the first three build jobs, it was higher for argon-silane atmosphere in build job 4 and 5. Averaged over all build jobs, there was no significant difference between the atmospheres. The mean horizontal roughness for argon atmosphere was 10.8  $\mu\text{m}$  and for argon-silane atmosphere 9.7  $\mu\text{m}$ . In addition, the horizontal roughness did not change significantly with increasing degree of recycling. Here, the high scatter both within a build job and between the build jobs must be taken into account. This can superimpose the effects of the varied parameters. In addition, the horizontal roughness is essentially determined by the laser parameters such as laser power, scanning speed and hatch strategy.

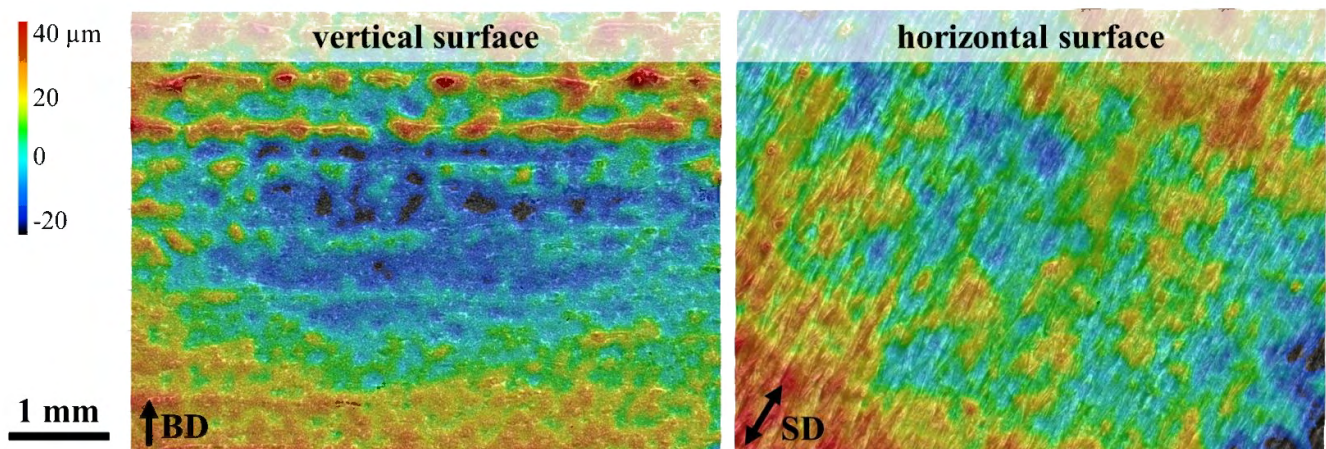


Fig. 3: Height profile of the vertical and horizontal surface with indicated build direction (BD) and scan direction (SD).

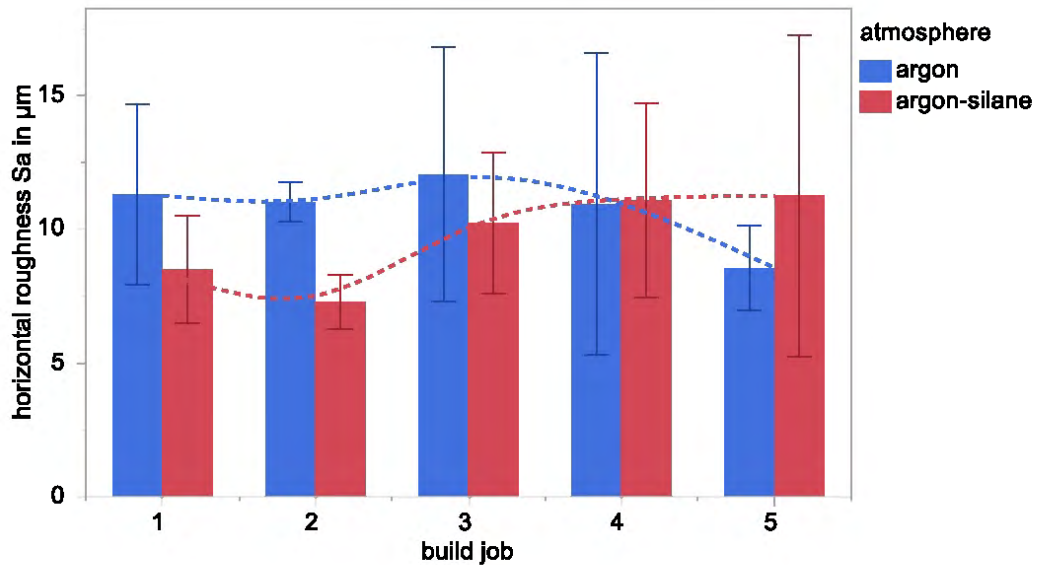


Fig. 4: Horizontal roughness Sa in dependence on build job number and atmosphere.

The vertical roughness in dependence on the build job number and atmosphere is displayed in Fig. 5. Here, a significant influence of the build job number on the vertical roughness could be observed, both for argon and argon-silane atmosphere. For argon, the vertical roughness is steadily increasing with increasing number of build jobs from 10.9 µm in the first build job to 13.4 µm in the fifth build job. The mean vertical roughness over all build jobs was 12.0 µm. Meanwhile, for argon-silane atmosphere there is first a drop of the vertical roughness within the first three build jobs. After that, the roughness also increases. The mean horizontal roughness was 14.5 µm in the first build job and 12.2 µm in the fifth build job. Over all build jobs, the mean roughness was 12.4 µm. While the drop in between cannot be explained by the known mechanisms and is likely due to the lack of reproducibility between build jobs, the increase of vertical surface roughness can be explained by the sintered powder adhesions. It is known that with increasing degree of powder recycling, the powder size distribution narrows and shifts toward larger mean particle size [2]. As a consequence, larger particles are sintered to the side surfaces of parts fabricated from recycled powder compared to the ones made of virgin powder. The high standard deviation due to the powder size distribution leads to the challenge of setting the roughness exactly to specified values.

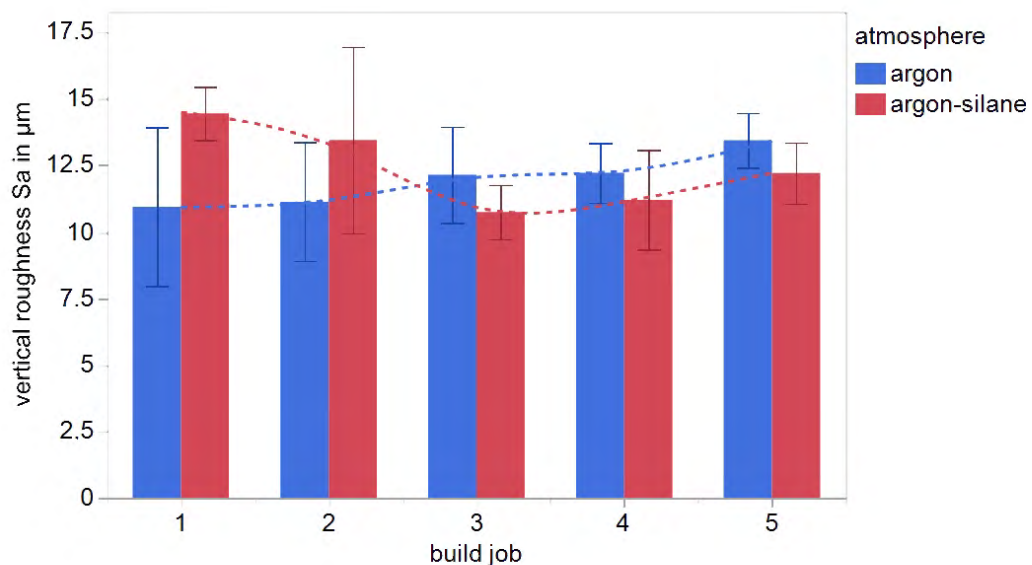


Fig. 5: Vertical roughness Sa in dependence on build job number and atmosphere.

## Relative density

Fig. 6 shows the mean relative density for the different build jobs and atmospheres. The mean relative density decreased significantly with increasing build job number for argon-silane atmosphere. However, also the standard deviation of the relative density increased strongly. For argon atmosphere, no significant change of the relative density after 5 build jobs could be observed. While the relative density was higher under argon-silane atmosphere for the first 3 build jobs, higher values were obtained for argon atmosphere for build job numbers 4 and 5. For argon atmosphere, the mean relative density slightly increases from 99.90 % in build job 1 to 99.93 % in build job 5. Meanwhile, the mean relative density for build job 1 under argon-silane atmosphere was 99.93 % and for build job 5 99.87 %. Since the standard deviation for argon silane-atmosphere is much higher than for argon atmosphere, it cannot be stated if one of the atmosphere leads to a better relative density after the 5 conducted build jobs. Thus, it is necessary to carry out more reusing cycles in future investigations. However, under both atmospheres a high density of over 99.9 % can be achieved even after multiple reusing cycles.

For both atmospheres, the observed pores were mainly spherical gas pores as shown exemplarily in the cross-section displayed in Fig. 7. In addition, there were occasional lack of fusion defects. This shows that under both atmospheres, the same porosity forming mechanisms are active for the chosen parameter settings.

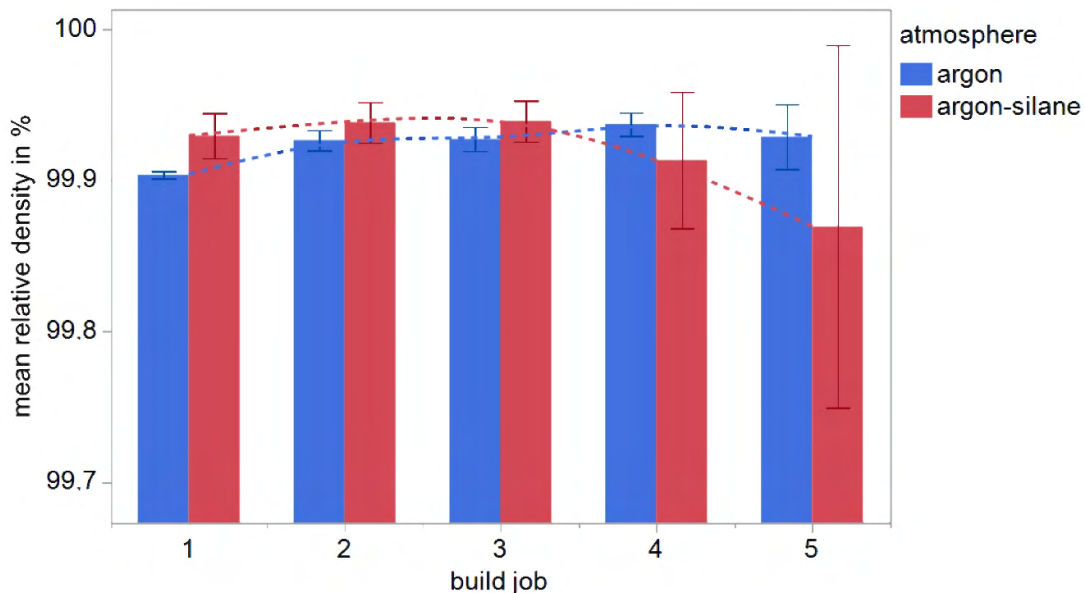


Fig. 6: Mean relative density in dependence on build job number and atmosphere.

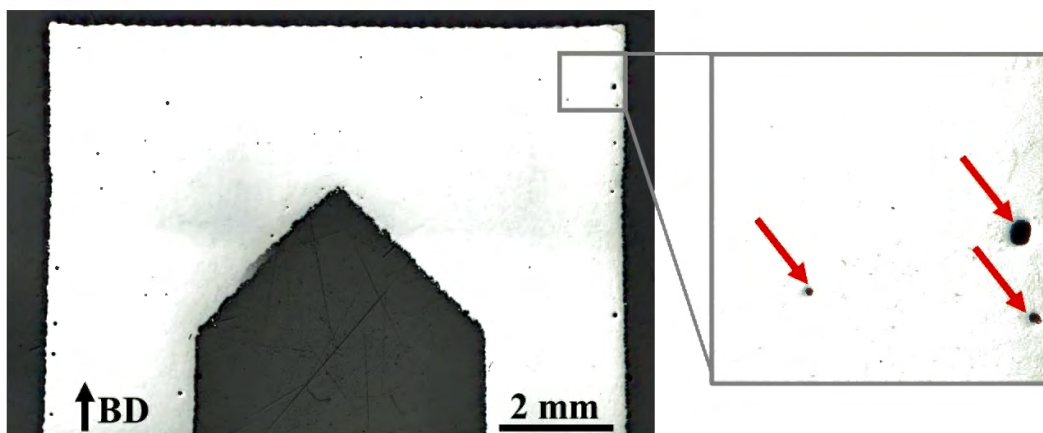


Fig. 7: Exemplarily cross-section of additively manufactured samples with gas pores (red arrows) and indicated build direction (BD).

## Powder characterization

The powder was characterized regarding its Hall flowability and apparent density right before the first build job, after three build jobs and sieving processes as well as after five build jobs and sieving processes. As shown in Fig. 8, the Hall flowability decreases and therefore improves continuously for increasing build job number. While it took 41 seconds for 50 g of the virgin powder to pass the Hall funnel it just took 39 s after 5 build jobs and sieving processes. The same trend was observed under both atmospheres. Regarding the apparent density, no significant change over five build jobs and sieving processes was observed for argon. For the virgin powder it was 2.28 g/mm<sup>3</sup> and after 5 build jobs it was also 2.28 g/mm<sup>3</sup>. In contrast, the apparent density for the powder processed under argon-silane atmosphere increased to 2.32 g/mm<sup>3</sup>. This can be linked to the improved flowability that leads to a closer packing of the powder particles and therefore a higher density.

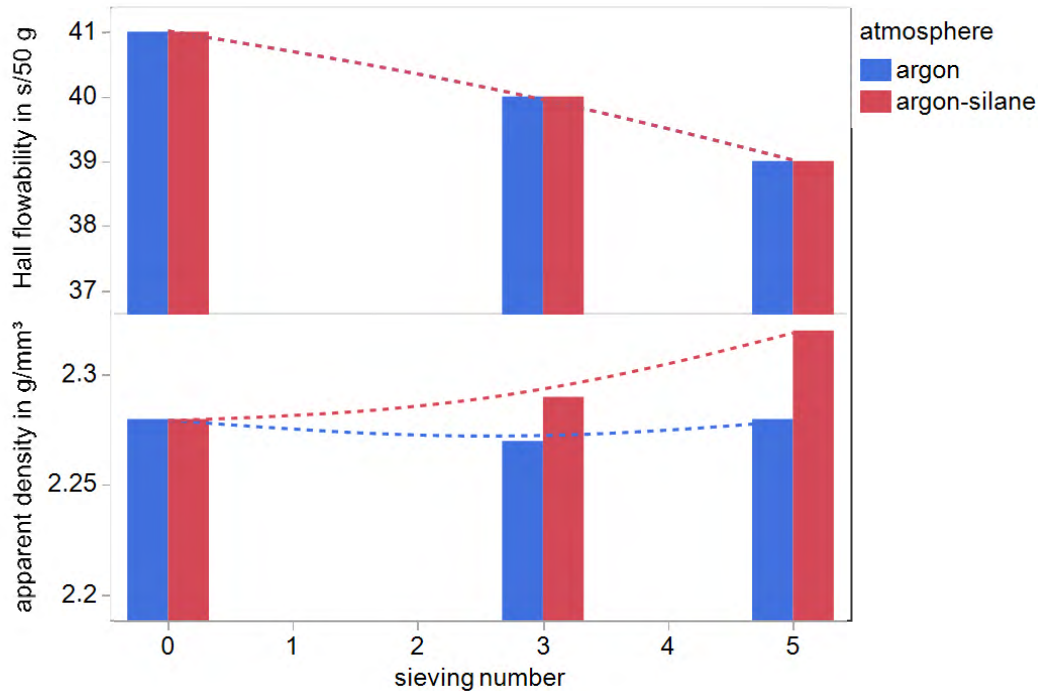


Fig. 8: Hall flowability and apparent density of the powder in dependence on build job number and atmosphere.

While the measured apparent density of the virgin powder is comparable to that given by the powder supplier, there is a significant difference in the values for the Hall flowability. This can be explained by the high dependence on the measurement method. The time that the powder took to flow through the Hall funnel was measured manually with a stopwatch and is therefore highly susceptible to examiner-dependent differences. However, when all measurements are conducted by the same person in the same way it allows for a good comparison between different measurements.

The powder characterization was also supplemented by SEM images and EDS measurements. Fig. 9 shows the SEM images of the powder after 5 build jobs and sieving processes for both atmospheres. No significant differences between the powder processed under argon and argon-silane atmosphere can be observed. Both powder samples consist of mainly spherical particles with only a few agglomerates. Additionally, there is still a high number of small satellite particles in both samples, comparable to the virgin powder, despite multiple build jobs and sieving processes. An increase of nanoparticles in the powder processed under argon-silane atmosphere due to potential deposition of formed silicon dioxide could not be detected.

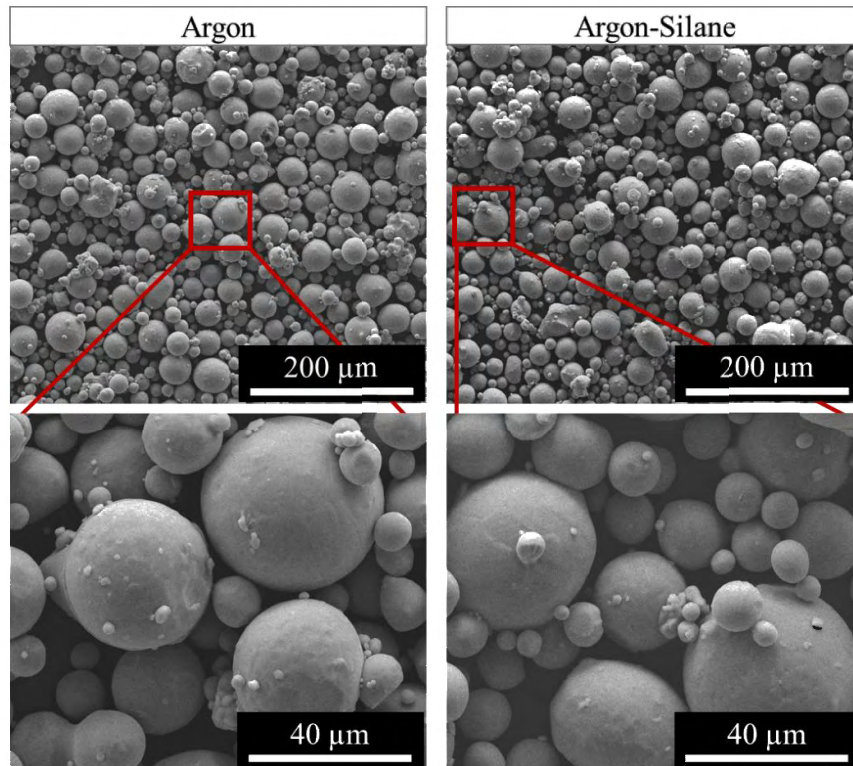


Fig. 9: SEM images of powder samples after five build jobs and sieving processes under argon and argon-silane atmosphere.

The EDS measurements (Table 1, 2 and 3) for the virgin powder as well as the powder processed 5 times under argon and argon-silane atmosphere are shown in Tables 1, 2 and 3, respectively. It can be seen, that the virgin powder contains the highest amount of titanium and aluminum. This can be explained by the partially evaporation and oxidation of these elements during processing. For the processed powder samples, the contents of titanium and the alloying elements vanadium and aluminum as well as silicon are comparable. For the powder processed under argon, a nearly three times higher oxygen content was measured compared to the powder processed under argon-silane atmosphere. However, the oxygen values for the processed powders (Table 2 and 3) are under the given minimum detection limit (MDL) and are therefore not reliable. In general, EDS measurements only allow qualitative comparisons. They could give a first hint that under a technically oxygen-free environment achieved by the argon-silane atmosphere less powder oxidation takes place. Powder in the direct vicinity of the process zone is heated up periodically and therefore is susceptible to critical oxidations. By eliminating the residual oxygen in the processing atmosphere, these oxidations could be significantly reduced resulting in a less severe degradation of the powder. However, this hypothesis needs to be verified by further investigations, especially inert gas fusion analysis.

Table 1: EDS measurement of virgin Ti-6Al-4V powder.

Element	Weight %	MDL	Atomic %	Error %
O K	2.7	1.53	7.4	29.7
Al K	5.0	0.12	8.1	8.5
Si K	0.2	0.1	0.3	37.2
Ti K	88.3	0.26	80.9	2.0
V K	3.9	0.98	3.4	5.8

Table 2: EDS measurement of Ti-6Al-4V powder processed 5 times under argon atmosphere.

Element	Weight %	MDL	Atomic %	Error %
O K	1.4	1.52	3.0	59.6
Al K	4.3	0.11	5.5	8.4
Si K	0.2	0.1	0.2	30.0
Ti K	79.8	0.22	57.6	2.0
V K	3.5	0.98	2.4	6.9

Table 3: EDS measurement of Ti-6Al-4V powder processed 5 times under argon-silane atmosphere.

Element	Weight %	MDL	Atomic %	Error %
O K	0.5	1.59	1.1	97.6
Al K	4.5	0.11	5.7	8.3
Si K	0.2	0.1	0.2	29.4
Ti K	79.4	0.27	56.9	2.0
V K	3.6	0.94	2.4	6.2

### Conclusions

In this work, Ti-6Al-4V powder was used for 5 L-PBF build jobs under argon as well as under silane-doped argon atmosphere and was sieved 5 times. The part properties horizontal and vertical roughness as well as the relative density were evaluated. Additionally, the powder properties Hall flowability and relative density were investigated and supplemented by SEM and EDS analysis of the powder. The following conclusions can be given:

- No significant effect of the atmosphere or the number of reusing cycles on the horizontal surface could be observed. The structure and roughness of this surface is mainly determined by the laser processing parameters and the high standard deviation of the surface quality represents a major challenge.
- The vertical surface roughness increases with increasing build job number. This is due to the powder coarsening resulting from the recycling of the powder. No influence of the atmosphere could be determined.
- The Hall flowability decreases and therefore improves with increasing amount of reusing cycles. No difference between the atmospheres was observed. Meanwhile, the apparent density increases under argon-silane atmosphere with increasing build job number while it remains unchanged under argon atmosphere.
- Regarding the SEM images of the virgin and recycled powders, no significant differences in morphology or qualitative size distribution could be seen. The EDS measurements shows higher amounts of titanium and aluminum in the virgin powder. No reliable statements regarding the oxygen content can be made since the measured values were below the minimum detection limit.

In general, the oxygen-free production using an argon-silane atmosphere is promising for obtaining high part qualities and longer powder lifetime. However, to clearly show this potential for powder recycling, a higher number of reusing cycles needs to be investigated. Besides that, future work will contain inert gas fusion analysis to quantify the amount of oxygen, nitrogen and hydrogen in the built parts as well as in the recycled powders. Finally, future work will contain the additional elimination of residual moisture beside the residual oxygen to unlock the full potential of an oxygen-free production.

## Acknowledgements

Funded by the Deutsche Forschungsgemeinschaft (DFG, German Research Foundation) – Project-ID 394563137 – SFB 1368.

## References

- [1] O. Geisen, J. Bogner, D. Rule, S. Purschke, M. Jurisch, Variable Layer Thicknesses in Laser Powder-Bed Fusion for Cost Reduction of a Gas Turbine Component, 2022.
- [2] E. Santecchia, S. Spigarelli, M. Cabibbo, Material Reuse in Laser Powder Bed Fusion: Side Effects of the Laser—Metal Powder Interaction, *Metals* 10 (2020) 341. <https://doi.org/10.3390/met10030341>.
- [3] A. Raza, C. Pauzon, E. Hryha, A. Markström, P. Forêt, Spatter oxidation during laser powder bed fusion of Alloy 718: Dependence on oxygen content in the process atmosphere, *Additive Manufacturing* 48 (2021) 102369. <https://doi.org/10.1016/j.addma.2021.102369>.
- [4] A. Raza, T. Fiegl, I. Hanif, A. Markström, M. Franke, C. Körner, E. Hryha, Degradation of AlSi10Mg powder during laser based powder bed fusion processing, *Materials & Design* 198 (2021) 109358. <https://doi.org/10.1016/j.matdes.2020.109358>.
- [5] T. Delacroix, F. Lomello, F. Schuster, H. Maskrot, C. Baslari, U. Gaumet, Y. Flici, J.-P. Garandet, Influence of build characteristics and chamber oxygen concentration on powder degradation in laser powder bed fusion, *Powder Technology* 416 (2023) 118231. <https://doi.org/10.1016/j.powtec.2023.118231>.
- [6] R. Williams, M. Bilton, N. Harrison, P. Fox, The impact of oxidised powder particles on the microstructure and mechanical properties of Ti-6Al-4 V processed by laser powder bed fusion, *Additive Manufacturing* 46 (2021) 102181. <https://doi.org/10.1016/j.addma.2021.102181>.
- [7] V. Seyda, N. Kaufmann, C. Emmelmann, Investigation of Aging Processes of Ti-6Al-4 V Powder Material in Laser Melting, *Physics Procedia* 39 (2012) 425–431. <https://doi.org/10.1016/j.phpro.2012.10.057>.
- [8] Renishaw plc, White paper: Investigating the effects of multiple re-use of Ti6Al4V powder in additive manufacturing (AM), 2016.
- [9] O.A. Quintana, J. Alvarez, R. Mcmillan, W. Tong, C. Tomonto, Effects of Reusing Ti-6Al-4V Powder in a Selective Laser Melting Additive System Operated in an Industrial Setting, *JOM* 70 (2018) 1863–1869. <https://doi.org/10.1007/s11837-018-3011-0>.
- [10] P.E. Carrion, A. Soltani-Tehrani, N. Phan, N. Shamsaei, Powder Recycling Effects on the Tensile and Fatigue Behavior of Additively Manufactured Ti-6Al-4V Parts, *JOM* 71 (2019) 963–973. <https://doi.org/10.1007/s11837-018-3248-7>.
- [11] R. O'Leary, R. Setchi, P. Prickett, G. Hankins, An Investigation into the Recycling of Ti-6Al-4V Powder Used Within SLM to Improve Sustainability, *InImpact: The Journal of Innovation Impact* 8 (2016) 377.
- [12] N. Derimow, N. Hrabe, Oxidation in Reused Powder Bed Fusion Additive Manufacturing Ti-6Al-4V Feedstock: A Brief Review, *JOM* 73 (2021) 3618–3638. <https://doi.org/10.1007/s11837-021-04872-y>.
- [13] W.A. Grell, E. Solis-Ramos, E. Clark, E. Lucon, E.J. Garboczi, P.K. Predecki, Z. Loftus, M. Kumosa, Effect of powder oxidation on the impact toughness of electron beam melting Ti-6Al-4V, *Additive Manufacturing* 17 (2017) 123–134. <https://doi.org/10.1016/j.addma.2017.08.002>.
- [14] O.A. Quintana, W. Tong, Effects of Oxygen Content on Tensile and Fatigue Performance of Ti-6Al-4 V Manufactured by Selective Laser Melting, *JOM* 69 (2017) 2693–2697. <https://doi.org/10.1007/s11837-017-2590-5>.
- [15] C. Pauzon, K. Dietrich, P. Forêt, S. Dubiez-Le Goff, E. Hryha, G. Witt, Control of residual oxygen of the process atmosphere during laser-powder bed fusion processing of Ti-6Al-4V, *Additive Manufacturing* 38 (2021) 101765. <https://doi.org/10.1016/j.addma.2020.101765>.
- [16] M. Velasco-Castro, E. Hernández-Nava, I.A. Figueroa, I. Todd, R. Goodall, The effect of oxygen pickup during selective laser melting on the microstructure and mechanical properties of Ti-6Al-4V lattices, *Heliyon* 5 (2019) e02813. <https://doi.org/10.1016/j.heliyon.2019.e02813>.

- [17] K. Dietrich, J. Diller, S. Dubiez-Le Goff, D. Bauer, P. Forêt, G. Witt, The influence of oxygen on the chemical composition and mechanical properties of Ti-6Al-4V during laser powder bed fusion (L-PBF), *Additive Manufacturing* 32 (2020) 100980. <https://doi.org/10.1016/j.addma.2019.100980>.
- [18] A. Raza, C. Pazon, S. Dubiez-Le Goff, E. Hryha, Effect of processing gas on spatter generation and oxidation of TiAl6V4 alloy in laser powder bed fusion process, *Applied Surface Science* 613 (2023) 156089. <https://doi.org/10.1016/j.apsusc.2022.156089>.
- [19] H. Amano, Y. Yamaguchi, T. Ishimoto, T. Nakano, Reduction of Spatter Generation Using Atmospheric Gas in Laser Powder Bed Fusion of Ti-6Al-4V, *Mater. Trans.* 62 (2021) 1225–1230. <https://doi.org/10.2320/matertrans.MT-M2021059>.
- [20] W.-H. Lee, T.-W. Na, K.-W. Yi, S.-M. Yang, J.-W. Kang, H.G. Kim, H.-K. Park, Thermodynamic analysis of oxidation during selective laser melting of pure titanium, *Rapid Prototyping Journal* 26 1401–1404. <https://doi.org/10.1108/RPJ-08-2019-0226>.
- [21] L. Wegewitz, W. Maus-Friedrichs, R. Gustus, H.J. Maier, S. Herbst, Oxygen-Free Production—From Vision to Application, *Adv Eng Mater* (2023) 2201819. <https://doi.org/10.1002/adem.202201819>.
- [22] U. Holländer, D. Wulff, A. Langohr, K. Möhwald, H.J. Maier, Brazing in SiH<sub>4</sub>-Doped Inert Gases: A New Approach to an Environment Friendly Production Process, *Int. J. of Precis. Eng. and Manuf.-Green Tech.* 7 (2020) 1059–1071. <https://doi.org/10.1007/s40684-019-00109-1>.
- [23] F. Tamanini, J.L. Chaffee, R.L. Jambor, Reactivity and ignition characteristics of silane/air mixtures, *Proc. Safety Prog.* 17 (1998) 243–258. <https://doi.org/10.1002/prs.680170405>.
- [24] P. Redhead, *Extreme High Vacuum: Tech. Rep.*, CERN, 1999.
- [25] N. Emminghaus, R. Bernhard, J. Hermsdorf, S. Kaierle, Laser-based powder bed fusion of Ti-6Al-4V powder modified with SiO<sub>2</sub> nanoparticles, *Int J Adv Manuf Technol* 122 (2022) 1679–1694. <https://doi.org/10.1007/s00170-022-09944-0>.
- [26] N. Emminghaus, S. Fritsch, H. Büttner, J. August, M. Tegtmeier, M. Huse, M. Lammers, C. Hoff, J. Hermsdorf, S. Kaierle, PBF-LB/M process under a silane-doped argon atmosphere: Preliminary studies and development of an innovative machine concept, *Advances in Industrial and Manufacturing Engineering* 2 (2021) 100040. <https://doi.org/10.1016/j.aime.2021.100040>.